



Original article

Photocytotoxic oxovanadium(IV) complexes of ferrocenyl-terpyridine and acetylacetonate derivatives

Babu Balaji^a, Babita Balakrishnan^b, Sravanakumar Perumalla^a, Anjali A. Karande^{b,*}, Akhil R. Chakravarty^{a,*}^a Department of Inorganic and Physical Chemistry, Indian Institute of Science, Sir C.V. Raman Avenue, Bangalore 560 012, India^b Department of Biochemistry, Indian Institute of Science, Sir C.V. Raman Avenue, Bangalore 560 012, India

ARTICLE INFO

Article history:

Received 1 August 2014

Received in revised form

8 November 2014

Accepted 3 January 2015

Available online 3 January 2015

Keywords:

Medicinal chemistry

Vanadium

Ferrocene

Photocytotoxicity

Cellular imaging

Apoptosis

ABSTRACT

Oxovanadium(IV) complexes [VO(Fc-tpy)(acac)](ClO₄) (**1**), [VO(Fc-tpy)(nap-acac)](ClO₄) (**2**), [VO(Fc-tpy)(py-acac)](ClO₄) (**3**) and [VO(Ph-tpy)(py-acac)](ClO₄) (**4**) of 4'-ferrocenyl-2,2':6',2''-terpyridine (Fc-tpy) and 4'-phenyl-2,2':6',2''-terpyridine (Ph-tpy) having monoanionic acetylacetonate (acac), naphthylacetylacetonate (nap-acac) or pyrenylacetylacetonate (py-acac) ligand were prepared, characterized and their photocytotoxicity in visible light studied. The ferrocenyl complexes **1–3** showed an intense charge transfer band near 585 nm in DMF and displayed Fc⁺/Fc and V(IV)/V(III) redox couples near 0.66 V and –0.95 V vs. SCE in DMF–0.1 M TBAP. The complexes as avid binders to calf thymus DNA showed significant photocleavage of plasmid DNA in green light (568 nm) forming •OH radicals. The complexes that are photocytotoxic in HeLa and MCF-7 cancer cells in visible light (400–700 nm) with low dark toxicity remain nontoxic in normal fibroblast 3T3 cells. ICP-MS and fluorescence microscopic studies show significant cellular uptake of the complexes. Photo-irradiation of the complexes causes apoptotic cell death by ROS as evidenced from the DCFDA assay.

© 2015 Elsevier Masson SAS. All rights reserved.

1. Introduction

Photodynamic therapy (PDT) which has emerged as a non-invasive treatment modality for various types of cancers using the FDA approved hematoporphyrin drug Photofrin[®] involves administration of the photosensitizer (PS) to the body, followed by its activation by light at the cancer site with formation of singlet oxygen killing the tumour cells [1–5]. The advantage of PDT over

other chemotherapeutic treatments is its selectivity to target only the photo-exposed cancerous cells leaving unexposed normal cells unaffected thus minimizing toxic side effects. Photofrin and its analogues suffer from prolonged skin photosensitivity and hepatotoxicity due to formation of bilirubin on oxidative degradation of the porphyrin core [6,7]. Non-porphyrinic transition metal complexes are shown to be efficient photocytotoxic agents with low dark toxicity [8–15]. The metal complexes could be suitably designed to show novel PDT activity following different reaction pathways, producing hydroxyl radicals or singlet oxygen to cause cellular damage [16,17].

We have recently shown that ferrocenyl conjugates of transition metals significantly enhance their photo-chemotherapeutic potential compared to the one lacking the ferrocenyl unit [18–20]. Ferrocenyl derivatives with their non-toxic, redox active and lipophilic properties have been used to prepare novel antitumor, antimalarial and antifungal agents [21–26]. Mechanistic studies have shown that the anticancer activity of the ferrocenium cation is due to generation of reactive oxygen species (ROS) including •OH radicals and these radicals are responsible for DNA degradation and strand-breakage [27]. We have also shown in a recent report that ferrocene-conjugated oxovanadium(IV) complexes of

Abbreviations: acac, acetylacetonate; ct-DNA, calf thymus DNA; DCFDA, 2',7'-dichlorofluorescein diacetate; DMEM, Dulbecco's Modified Eagle's Medium; DMF, dimethylformamide; DMSO, dimethyl sulfoxide; DNA, deoxyribonucleic acid; DPPH, 2,2-diphenyl-1-picrylhydrazyl; EB, ethidium bromide; EDTA, ethylenediaminetetraacetate; EPR, electron paramagnetic resonance; FBS, fetal bovine serum; Fc, ferrocenyl; Fc-tpy, 4'-ferrocenyl-2,2':6',2''-terpyridine; ICP-MS, inductively coupled plasma mass spectrometry; MLCT, metal-to-ligand charge transfer; MTT, 3-(4,5-dimethylthiazol-2-yl)-2,5-diphenyltetrazolium bromide; MvH, McGhee-von Hippel; NAC, N-acetylcysteine; nap-acac, naphthylacetylacetonate; PBS, phosphate buffered saline; PDT, photodynamic therapy; Ph-tpy, 4'-phenyl-2,2':6',2''-terpyridine; PI, propidium iodide; py-acac, pyrenylacetylacetonate; ROS, reactive oxygen species; TBAP, tetrabutylammonium perchlorate.

* Corresponding authors.

E-mail addresses: anjali@biochem.iisc.ernet.in (A.A. Karande), arc@ipc.iisc.ernet.in (A.R. Chakravarty).

curcuminoids are photocytotoxic in cancer cells [28]. Curcumin has a dione moiety which in its enolized form resembles the metal binding properties of acetylacetonates [29]. The present work stems from our interests to extend this chemistry further by using different acetylacetonate derivatives in a ternary structure in which the oxovanadium(IV) moiety is bound to a tridentate ferrocenylterpyridine ligand and a bidentate acetylacetonate derivative. Curcumin with its poor bioavailability is known to be susceptible to hydrolytic degradation in the physiological medium [30]. In contrast, the acac ligands are expected to be of higher stability in a biological medium. The acac derivatives bearing fluorophoric pendants like naphthyl or pyrenyl moiety could be used to study the cellular localization of the complexes by fluorescence microscopy. The 4'-ferrocenyl-2,2':6',2''-terpyridine (Fc-tpy) ligand with its intense charge transfer band is used as a photosensitizer.

Herein, we report the synthesis, characterization, photocytotoxicity and cellular imaging of ferrocenyl-terpyridine (Fc-tpy) oxovanadium(IV) complexes of acetylacetonate derivatives, viz. $[\text{VO}(\text{Fc-tpy})(\text{acac})](\text{ClO}_4)$ (**1**), $[\text{VO}(\text{Fc-tpy})(\text{nap-acac})](\text{ClO}_4)$ (**2**), $[\text{VO}(\text{Fc-tpy})(\text{py-acac})](\text{ClO}_4)$ (**3**) and $[\text{VO}(\text{Ph-tpy})(\text{py-acac})](\text{ClO}_4)$ (**4**), where acac is acetylacetonate, nap-acac is naphthylacetylacetonate and py-acac is pyrenylacetylacetonate (Scheme 1). Complex **4** having the ferrocenyl moiety replaced by a phenyl group was used as a control. Significant results of this study include remarkable photocytotoxicity of the py-acac complexes and cytosolic localization of complex **3** as evidenced from the fluorescence microscopy imaging study. The pyrenyl complex shows similar photocytotoxicity as observed for its reported curcumin analogue [28].

2. Results and discussion

2.1. Chemistry

The terpyridine ligands (Fc-tpy and Ph-tpy) were prepared by reacting corresponding aldehyde with 2-acetylpyridine and NaOH with subsequent condensation of the intermediate species with ammonium acetate in refluxing ethanol [31]. The 1-naphthylacetylacetonate (Hnap-acac) and pyrenylacetylacetonate (Hpy-acac) were prepared by following a literature procedure [32]. 1-Acetylnaphthalene or 1-acetylpyrene was refluxed with sodium sand in dry ethyl acetate for 4 h and poured into cold water. The aqueous layer was acidified with dilute HCl to precipitate out the

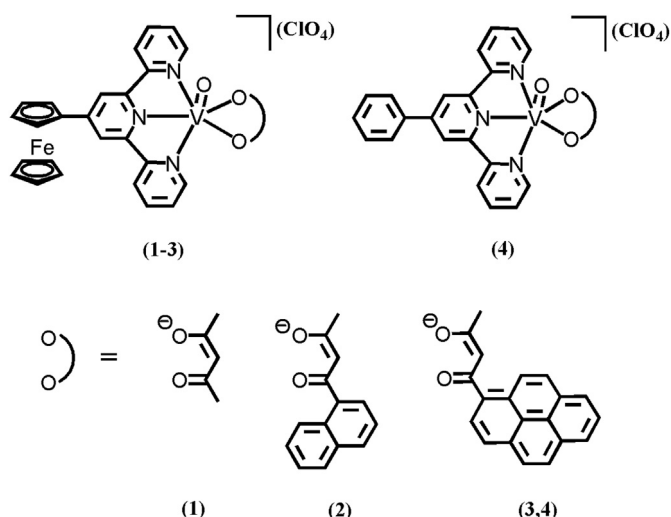
product. The metal precursor vanadyl perchlorate was prepared by reacting vanadyl sulphate with calcium perchlorate. Oxovanadium(IV) complexes **1–4** were prepared by a general synthetic method in two steps. First, the acetylacetonate derivative after neutralizing with dilute NaOH was reacted with vanadyl perchlorate for 30 min. Corresponding terpyridine ligand in $\text{CHCl}_3\text{--MeOH}$ was then added and stirred for further 30 min. The complex was isolated as its perchlorate salt.

2.2. Pharmacology

Photocytotoxicity of the oxovanadium(IV) complexes **1–4** in HeLa and MCF-7 cells was evaluated by MTT assay in dark and visible light (400–700 nm). The cellular uptake of the complexes was evaluated by ICP-MS. The cellular localization studies were carried out by fluorescence microscopy using the blue fluorescence of the naphthyl and pyrenyl groups present in the complexes. The mechanism of cell death on photo-irradiation was assessed by Hoechst staining. The generation of reactive oxygen species (ROS) in the cells on photo-irradiation was evaluated by DCFDA assay. The oxovanadium(IV) complexes were also evaluated for their calf thymus DNA binding strengths and plasmid DNA photocleavage activities. The DNA binding studies were done by spectroscopic methods, viz. electronic absorption titration, DNA melting and viscosity measurements. The DNA cleavage activity of the complexes was studied using plasmid supercoiled (SC) form of DNA. The extent of DNA cleavage forming nicked circular (NC) DNA was quantified by gel electrophoresis.

2.3. Synthesis and general aspects

Complexes $[\text{VO}(\text{Fc-tpy})(\text{L})](\text{ClO}_4)$ (**1–3**) of acetylacetonate derivatives (L: acac in **1**; nap-acac in **2**; py-acac in **3**) and the ferrocenyl terpyridine ligand (Fc-tpy) were prepared in good yield. Complex **4** was prepared using Ph-tpy instead of Fc-tpy and used as a control species. Complexes **1–4** were characterized from the analytical, mass spectral and other physicochemical data (Table 1). The molar conductance value of $\sim 82 \text{ S m}^2 \text{ M}^{-1}$ of the complexes in DMF at 25 °C suggests their 1:1 electrolytic behaviour. The ESI mass spectra of the complexes in MeCN showed a single peak corresponding to the molecular ion peak (m/z) as $[\text{VO}(\text{Fc-tpy})(\text{L})]^+$. The isotopic distribution pattern of the complexes is in accordance with the calculated one. The IR spectra of the complexes in the solid state showed C=O and C=C bands that are shifted to lower wavenumbers compared to the free ligands due to binding to the metal. The complexes showed band for V=O and ClO_4^- within 958–963 cm^{-1} and 1090–1096 cm^{-1} , respectively [33]. The $3d^1\text{-VO}^{2+}$ complexes are one-electron paramagnetic giving a magnetic moment value of $\sim 1.64 \mu_B$. The complexes showed broad $^1\text{H NMR}$ spectra due to their paramagnetic nature. The complexes showed eight line pattern in the ESR spectra due to hyperfine coupling of the unpaired electron with the ^{51}V nucleus ($I = 7/2$), confirming the $3d^1\text{-VO(IV)}$ oxidation state. Complexes **1–3** showed an intense band at $\sim 585 \text{ nm}$ which is assignable to the metal to ligand charge transfer transition (MLCT) (Fig. 1) [34]. This band is absent in the spectrum of the phenyl analogue **4** indicating the involvement of the ferrocenyl moiety for this charge transfer transition. Complex **4** showed only a weak d–d transition at 774 nm. The d–d band in **1–3** was found to be masked by the MLCT band. The complexes **2–4** showed fluorescence property (Fig. 1). Complex **2** having a naphthyl moiety showed emission bands at 406 and 430 nm, while the pyrenyl complexes **3** and **4** showed emission bands at 387 and 409 nm, respectively. Cyclic voltammetry of the redox active complexes in DMF-0.1 M TBAP showed quasi-reversible Fc^+/Fc redox couple near 0.62 V (Fc = ferrocenyl unit) and the V(IV)/V(III)



Scheme 1. Schematic drawings of the complexes **1–4** and ligands used.

Table 1
Selected physicochemical and DNA binding data for the complexes **1–4**.

Complex		1	2	3	4
IR/cm ⁻¹ (in KBr)	v (V=O)	958	958	960	961
	v (ClO ₄)	1096	1095	1096	1095
$\lambda_{\text{max}}/\text{nm}$ ($\epsilon/\text{dm}^3 \text{M}^{-1} \text{cm}^{-1}$) ^a		581 (2608)	583 (3014)	586 (3536)	777 (90)
E_f/V ($\Delta E_p/mV$) ^b		0.62 (170)	0.63 (155)	0.62 (165)	–
Fc ⁺ –Fc ^c					
E_p [V] ^d		–0.93	–0.98	–1.01	–0.97
$\Lambda_M^e/S \text{m}^2 \text{M}^{-1}$		84	86	79	74
g_{iso}^f		1.99	1.98	1.98	1.98
K_b^g		$(4.5 \pm 0.5) \times 10^4$	$(3.2 \pm 0.3) \times 10^5$	$(9.6 \pm 0.4) \times 10^5$	$(3.8 \pm 0.3) \times 10^6$
ΔT_m^h (°C)		1.1	2.6	4.9	4.4

- ^a Visible electronic spectral band in DMF–Tris HCl buffer (1:1 v/v).
^b Redox data in DMF–0.1 M TBAP. The potentials are vs. SCE. Scan rate = 50 mV s⁻¹. $E_f = (E_{pa} + E_{pc})/2$, $\Delta E_p = (E_{pa} - E_{pc})$, where E_{pa} and E_{pc} are the anodic and cathodic peak potentials, respectively.
^c Fc⁺/Fc redox couple.
^d Cathodic peak for the V^{IV}–V^{III} redox couple.
^e Molar conductance in DMF at 25 °C.
^f From room-temperature EPR spectra in DMF solution with DPPH as an internal standard.
^g Intrinsic equilibrium DNA binding constant from the UV–visible experiment.
^h Change in the calf thymus DNA melting temperature.

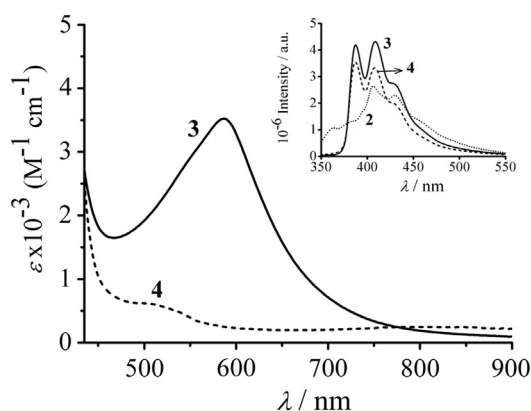


Fig. 1. The electronic spectra of [VO(Fc-tpy)(py-acac)](ClO₄) (**3**) (—) and [VO(Ph-tpy)(py-acac)](ClO₄) (**4**) (---) in DMF–Tris–HCl buffer (1:1 v/v) with the inset showing the emission spectrum of **2–4** in DMF.

couple as an irreversible reduction in the range from –0.91 to –0.97 V. Complex **4** showed only the V(IV)–V(III) reduction peak at –0.98 V.

In order to gain more detailed insight into the photophysical properties of the complexes, density functional theory (DFT) and its time-dependent version (TDDFT) were applied and the details are presented as Supporting Information [35–37]. The calculated absorption band positions for **1–3** at 600 nm are responsible for the experimentally observed intense band at ~585 nm. This absorption is associated with charge transfer from the HOMO to LUMO orbital for **1** and **2**, while it is HOMO–1 to LUMO orbital of **3** (Fig. 2). No such band was observed for the phenyl analogue **4**. The HOMO of **1** and **2** and HOMO–1 of **3** have predominant contribution from the ferrocenyl moiety (~97%). The LUMO has a major contribution from the terpyridine (tpy) moiety (~83%) and some V=O character (~9%). The metal-to-ligand charge-transfer (MLCT) is from the ferrocenyl to the terpyridine moiety in the complex. The TDDFT data are in agreement with the experimental results.

2.4. Stability of the complexes

The stability of the complexes was studied in 1% DMSO-PBS buffer (pH = 7.2) using UV-Visible spectroscopic technique. There was no change in the spectral features of the complexes in 24 h

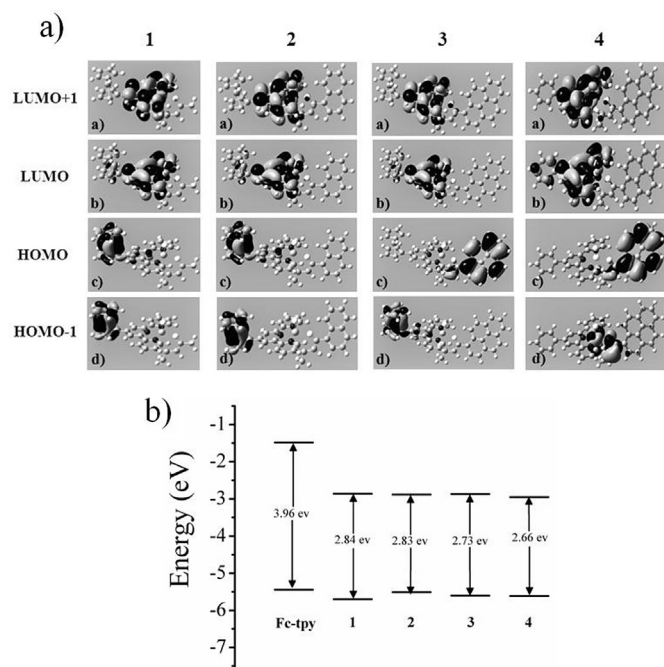


Fig. 2. Frontier orbital diagram of complexes **1–4** showing a) HOMO, HOMO–1, LUMO, LUMO+1 and b) the HOMO–LUMO energy gap of the ligand (Fc-tpy) and the complexes **1–4**.

indicating the solution stability of the complexes. The inertness of ferrocene moiety in complexes **1–3** in dark is established by monitoring the cyclic voltammograms of Fc–Fc⁺ couple in complexes with time. The cyclic voltammograms remained the same over the period of 4 h indicating ferrocenyl moiety not undergoing any oxidation when kept in dark. The ⁵¹V NMR of complex **3** in dark with time showed no peaks in spectra due to paramagnetic V(IV) moiety in **3**. This suggests that the complex not undergoing any oxidation to give diamagnetic V(V) species which is ⁵¹V NMR active.

2.5. Photocytotoxicity

The photocytotoxicity of the complexes **1–4** in cervical HeLa cancer and breast MCF-7 cancer cells and in normal fibroblast 3T3

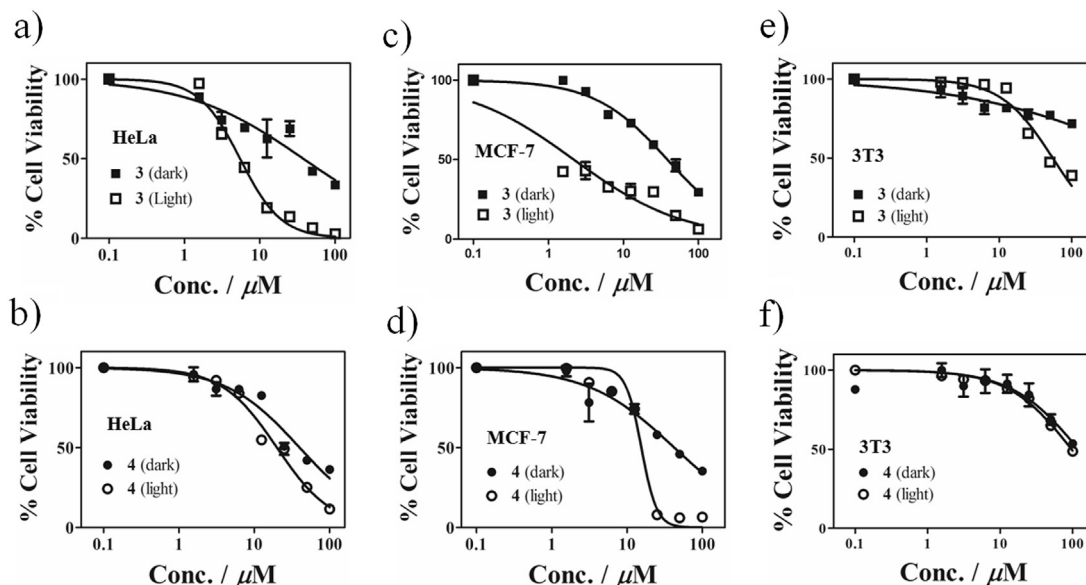


Fig. 3. MTT assay showing photocytotoxicity of **3** and **4** in HeLa (a, b) and MCF-7 (c, d) cancer cells and in normal 3T3 cells (e, f) on 4 h incubation in dark (with black symbol) and on photo-irradiation with visible light of 400–700 nm (shown as open circle), as determined from the MTT assay.

cells was studied in dark and visible light (400–700 nm) by MTT assay (Fig. 3). To optimize the incubation time of the complexes, MTT assay was done in HeLa cells by varying the incubation time to 2, 4, 6 and 8 h using complex **3**. Cellular uptake of complex **3** into the cancer cells was studied by FACS analysis which showed that **3** was taken up significantly within 4 h of incubation with the HeLa cells and remained the same after 6 or 8 h. It was also observed that increasing the incubation time resulted in an increase in the dark toxicity and a 4 h incubation showed better photocytotoxicity. Based on these results, a 4 h incubation period was chosen before photo-irradiating the samples with visible light of 400–700 nm (10 J cm^{-2}) to obtain the IC_{50} values of the complexes. The complexes were found to be significantly photocytotoxic compared to

their activity in dark. The IC_{50} values for the complexes are given in Table 2 along with few related compounds [38–42]. The ferrocenyl complex **3** showed better photocytotoxicity than its phenyl analogue **4** with IC_{50} values of 5.4 and 2.1 μM in HeLa and MCF-7 cells, respectively. This difference could be attributed to the presence of an MLCT band in complex **3** in the visible region (590 nm) which is absent in complex **4**. We have thus observed an improved photocytotoxicity on incorporating the ferrocenyl organometallic moiety. The complexes in general showed better activity in MCF-7 cells than in HeLa cells. In order to see the selectivity of the complexes from cancerous to the normal cells, we did MTT assay using normal fibroblast 3T3 cell line. Interestingly, the complexes showed 10 times less photocytotoxicity in normal 3T3 cells compared to the

Table 2

IC_{50} values of **1–4** with other relevant compounds in HeLa and MCF-7 cancer cells and in normal 3T3 fibroblast cell.

Compound	HeLa		MCF-7		3T3	
	IC_{50} (μM) dark ^a	IC_{50} (μM) light ^b	IC_{50} (μM) dark ^a	IC_{50} (μM) light ^b	IC_{50} (μM) dark ^a	IC_{50} (μM) light ^b
1	40.2 (± 1.1)	24.4 (± 1.1)	41.2 (± 1.0)	5.6 (± 0.9)	>100	66.8 (± 1.1)
2	45.1 (± 1.2)	15.5 (± 1.0)	48.7 (± 1.1)	3.3 (± 0.6)	>100	60.5 (± 1.0)
3	37.6 (± 1.2)	5.4 (± 0.5)	38.5 (± 1.1)	2.1 (± 0.3)	>100	54.5 (± 1.0)
4	40.1 (± 1.1)	19.9 (± 1.1)	42.4 (± 1.1)	15.5 (± 1.2)	>100	96.7 (± 2.1)
Fc-tpy ligand	>100	39.3 (± 1.8)	>100	32.4 (± 1.3)	>100	>100
[VO(Fc-tpy)(dppz)](ClO ₄) ₂ ^c	35.5 (± 1.0)	13.4 (± 1.1)	–	–	–	–
[VO(Fc-pic)(Curc)](ClO ₄) ₂ ^d	34.7 (± 1.9)	17.8 (± 1.2)	–	–	–	–
[VO(Fc-tpy)(Curc)](ClO ₄) ₂ ^e	54.2 (± 1.1)	2.4 (± 0.3)	–	–	46.4 (± 1.5)	22.5 (± 1.1)
[VOCl(dppz) ₂](ClO ₄) ^f	>100	12.0	–	–	–	–
Photofrin ^{®g}	>41	4.28	–	2.0 (± 0.2) ^h	–	–
Cisplatin	71.3 (± 2.9) ⁱ	68.7 (± 3.4) ^j	2.0 (± 0.3) ^j	–	–	–

^a The IC_{50} values for complexes **1–4** and ligands correspond to 4 h incubation in the dark without any photoexposure. The IC_{50} values for ligands in all the above three cell lines are given as Supplementary data.

^b The IC_{50} values of complexes **1–4** and ligands correspond to 4 h incubation in the dark followed by photoexposure to visible light (400–700 nm, 10 J cm^{-2}) for 1 h.

^c The IC_{50} values are from Ref. [18].

^d The IC_{50} values are from Ref. [29].

^e The IC_{50} values are from Ref. [28].

^f The IC_{50} values are from Ref. [38].

^g The Photofrin[®] IC_{50} values (633 nm excitation; fluence rate: 5 J cm^{-2}) are taken from Ref. [39] (converted to μM using the approximate molecular weight of Photofrin[®], 600 g M^{-1}).

^h The Photofrin[®] IC_{50} values (2 h exposure; white bulb; fluence rate: $5.5 \times 10^{-2} \text{ mW cm}^{-2}$) are taken from Ref. [40].

ⁱ The IC_{50} values for 4 h treatment are taken from Ref. [41].

^j The IC_{50} values for 96 h treatment are taken from Ref. [42].

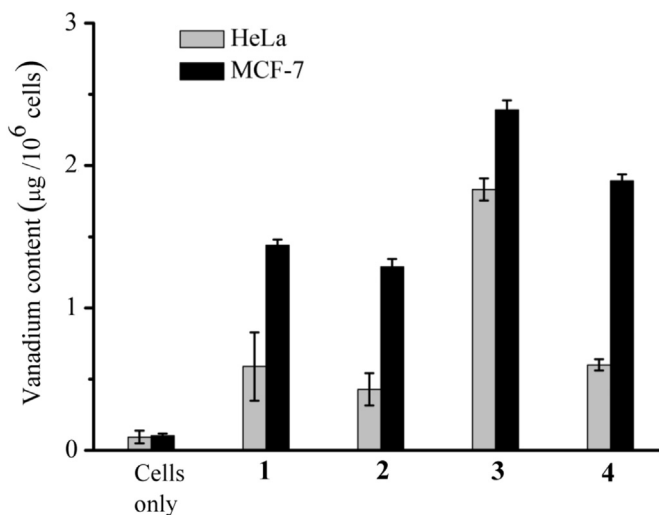


Fig. 4. Cellular vanadium content as determined by ICP-MS in HeLa and MCF-7 cancer cells upon incubation with the complexes **1–4** (30 µM) at 37 °C for 4 h.

cancerous ones (HeLa, MCF-7) and remained inactive in dark. The complexes are thus active against only the cancerous cells leaving the normal cells unaffected. When photo-irradiation was done in the presence of N-acetyl cysteine as a ROS scavenger, the activity of the complexes decreased significantly in both the cells indicating possible involvement of ROS in the cellular damage.

2.6. Cellular uptake from ICP-MS

The observed difference in the photocytotoxic activity of the complexes among the cancer cells could be related to their cellular uptake. The vanadium content associated with the cancer cells upon incubation for 4 h in dark with complexes **1–4** (30 µM) at 37 °C was measured by ICP-MS (Fig. 4). The DMSO (1% in DMEM media) treated cells were used as a control. The uptake of the complexes follows the order: **3** > **4** > **1** > **2** in both the cell lines with better uptake in MCF-7 compared to HeLa cells. The ferrocenyl complex **3** ($1.83 \pm 0.07 \mu\text{g}/10^6$ cells in HeLa, $2.39 \pm 0.07 \mu\text{g}/10^6$ cells in MCF-7) showed better cellular uptake than its phenyl analogue **4** ($0.60 \pm 0.04 \mu\text{g}/10^6$ cells, $1.89 \pm 0.05 \mu\text{g}/10^6$ cells) (Table 3). This could be due to higher lipophilic nature of the ferrocenyl moiety present in complex **3**.

2.7. Measurement of intracellular ROS

Generation of any reactive oxygen species (ROS) by the complexes (10 µM) was examined by dichlorofluorescein diacetate (DCFDA) assay. DCFDA is a cell permeable fluorogenic probe that on

Table 3

Uptake of the oxovanadium(IV) complexes (**1–4**) by HeLa and MCF-7 cells after 4 h incubation by ICP-MS.

Compound	Vanadium content ^a (µg/10 ⁶ cells)	
	HeLa cells	MCF-7 cells
Cells alone	0.09 ± 0.04	0.10 ± 0.01
1	0.59 ± 0.30	1.44 ± 0.04
2	0.43 ± 0.10	1.29 ± 0.06
3	1.83 ± 0.07	2.39 ± 0.07
4	0.60 ± 0.04	1.89 ± 0.05

^a Total accumulation of vanadium in HeLa and MCF-7 cells for complexes **1–4** after 4 h at 37 °C.

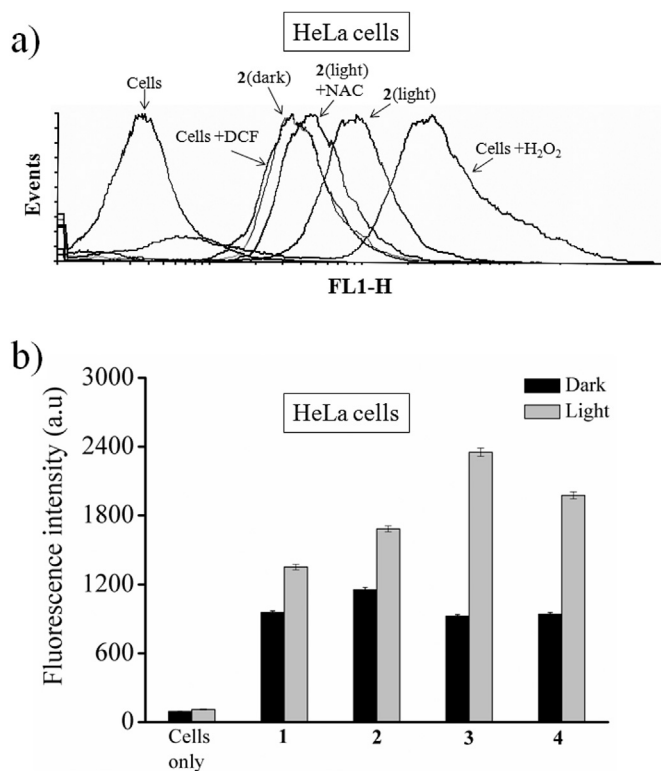


Fig. 5. a) DCFDA assay used for ROS generation in HeLa cells by complex **2** (10 µM) on exposure to visible light (400–700 nm). b) A comparison of the DCF derived fluorescence intensity of the cells treated with complexes **1–4** in dark and light.

oxidation forms 2',7'-dichlorofluorescein (DCF) showing an emission maximum at 528 nm. The assay was done by fluorescence-activated cell sorting (FACS) method in which the cancer cells on treatment with the complexes (10 µM) showed a significant positive shift in the fluorescence intensity due to formation of DCF in the presence of ROS generated on photo-irradiation of the complexes (Fig. 5). To verify further the ROS mediated cytotoxicity, the cancer cells were treated with complex **2** and N-acetyl-L-cysteine (NAC) as ROS quencher followed by photo-irradiation with visible light [43]. The fluorescence intensity was found to reduce in presence of NAC. The results indicate that the complexes generate ROS in the cellular medium only upon photo-irradiation but not in the dark. The positive control cells (H₂O₂ treated cells) showed a significant shift compared to the control cells. A comparison of the DCF derived fluorescence intensity of the cells treated with complexes **1–4**, the production of ROS follows the order: **3** > **4** > **2** > **1**. This trend could be related to the higher cellular uptake of complex **3** than the other complexes.

2.8. Fluorescence microscopy

Fluorescence microscopic study was done to visualize the localization of the complexes in the cells using the emission property of the pyrenyl and naphthyl moieties. The ICP-MS analysis showed that the complexes were taken up effectively into the cells. HeLa cells, on treatment with complex **3** for different time intervals (2 and 4 h), showed preferential uptake and it localized predominantly in the cytosol as seen from the blue fluorescence of **3** in panels (e) and (h) of Fig. 6. MCF-7 cells treated with complex **3** showed the same trend of cytosolic localization. It is evident that there is not much difference in the fluorescence intensity of the cells treated with **3** in 2 and 4 h time point. This is in agreement

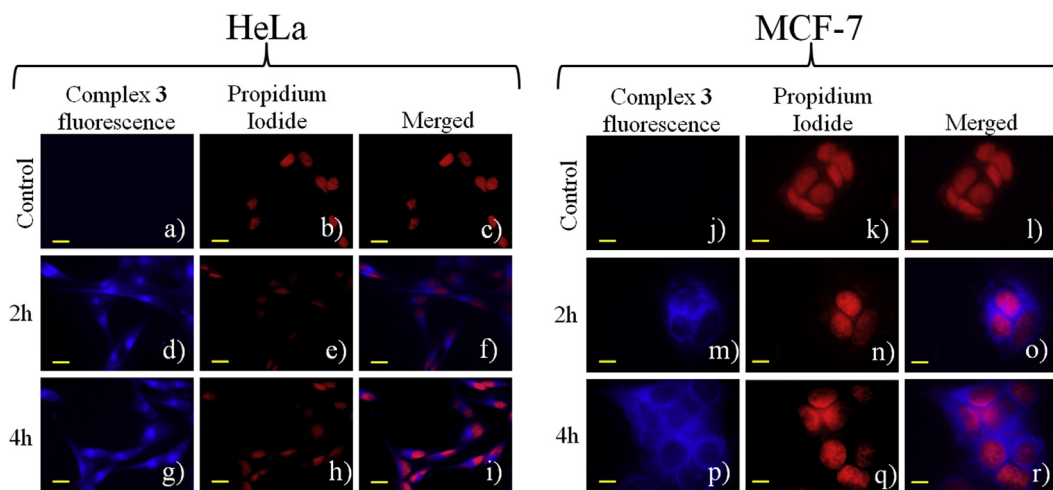


Fig. 6. A time-course collection of fluorescence microscopic images of untreated control cells (panels: a–c and j–l), [VO(Fc-tpy)(py-acac)](ClO₄) (**3**) (10 μM) in HeLa and MCF-7 cells. Panels (d), (g), (m) and (p) show the blue emission of **3**. Panels (b), (e), (h), (k), (n) and (q) correspond to the red emission of propidium iodide (PI) dye. Panels (c), (f), (i), (l), (o) and (r) display the merged images of the first two panels. Scale bar = 20 μm. (For interpretation of the references to colour in this figure legend, the reader is referred to the web version of this article.)

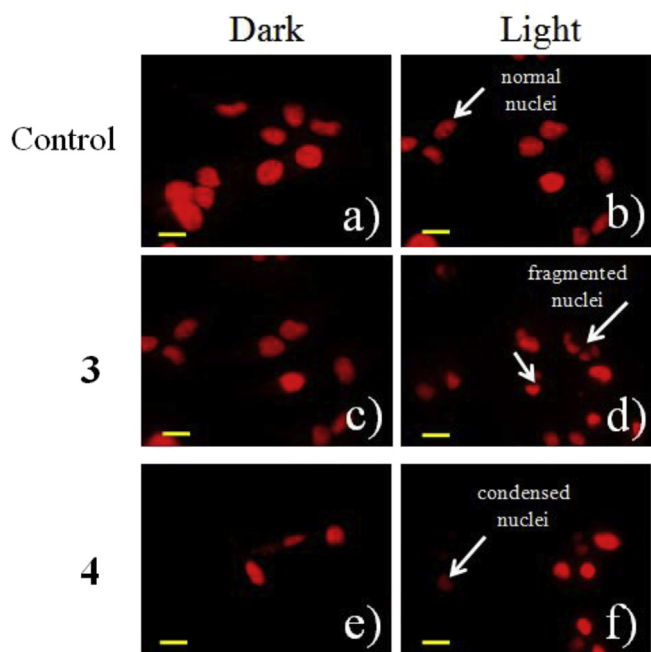


Fig. 7. Propidium iodide (PI) staining of the HeLa cells treated with complexes **3** and **4** for 4 h incubation in dark followed by light exposure to visible light (400–700 nm, 10 J cm⁻²) for 1 h. Panels (a), (c) and (e) are the fluorescence images of the control, complexes **3** and **4** treated cells (PI stained) in dark respectively. Panels (b), (d) and (f) are the fluorescence images of the control and complexes **3**, **4** treated cells in light respectively. The PDT effect is shown by arrows in panels (d) and (f). The scale bar is 20 μm.

with the cellular uptake results of complex **3** by FACS. Staining with PI which specifically stains the nucleus revealed minor localization of the complex within the nucleus (panels (f), (i), (o) and (r)). Cells treated with the complexes **2** and **4** showed similar cellular localization as observed for complex **3**.

To see the PDT effect, complexes **3** and **4** (10 μM) were added to the HeLa cells and incubated for 4 h in dark followed by exposure to visible light of 400–700 nm for 1 h (Fig. 7). Fluorescence images of the cells incubated with the complex on visible light exposure

showed nuclear fragmentation, chromatin condensation indicating apoptotic cell death (Fig. 7, panels (d), (f)). But nuclei of the cells when kept in dark for 4 h with complexes **3** and **4** were found to be healthy (Fig. 7, panels (a), (c), (e)). The results suggest that cell death occurred only in light with no apparent cell death in the dark.

2.9. Mechanistic aspects

To identify the possibility of formation of any hydroxyl radical as ROS by the complexes on photo-irradiation, EPR spin trapping was done using DMPO as a spin trap. Photo-irradiation of complex **3** (100 μM) in 10% DMSO-Tris HCl buffer with visible light in the presence of 5,5-dimethyl-1-pyrroline-N-oxide (DMPO) (100 mM) for 30 min gave a four line EPR spectrum which corresponds to DMPO-OH adduct with a hyperfine splitting of $a_N = a_H = 14.9$ Gauss [44]. No such EPR signal was observed when complex **4** was treated with DMPO in dark. Addition of superoxide dismutase (SOD) prior to irradiation led scavenging of the ROS. No DMPO-OH adduct formation was noticed in the presence of catalase. The reduction of DMPO-OH formation by SOD is possibly due to formation of unstable DMPO-O₂⁻ spin adduct with reduced life time [45]. The effect of catalase addition indicates formation of H₂O₂ in the photochemical reaction. The results suggest oxidation of the ferrocenyl moiety to ferrocenium ion on light activation and the ferrocenium ion which being unstable in a buffer medium degrades to form the hydroxyl radicals [46,47]. The involvement of the Fc unit undergoing oxidation on photo-irradiation was evidenced from the spectral studies showing the absorption maximum shifting to 590 nm with an increase of the intensity of that band with time [20]. A similar spectral change was noticed when complex **3** was oxidized chemically by ceric(IV) ammonium nitrate. Complex **4** lacking the ferrocenyl moiety did not show any such spectral change.

2.10. DNA binding and photocleavage

Since the complexes showed partial localization within the nucleus of the cells where DNA could be the possible target for observed cytotoxicity, we studied the DNA binding and photocleavage properties of the complexes. The ct-DNA binding studies were carried out by UV-visible absorption titration, DNA melting

and viscometric methods. Selected DNA binding data are given in Table 1. UV–Vis absorption titration method was used to determine the intrinsic DNA binding constant (K_b) of the complexes by monitoring the change in the absorption intensity of the ligand-centred band of the complexes **1–4** at ~ 280 nm. The complexes showed significant hypochromicity. The K_b values were in the range of 10^4 – 10^6 M^{-1} following the order: **3** > **4** > **2** > **1**. The binding data suggest partial intercalative binding mode of the complexes **3** and **4** having planar aromatic moieties, while complexes **1** and **2** have surface and/or partial groove binding to ct-DNA. Thermal DNA denaturation experiments showed a positive shift in the DNA melting temperature (ΔT_m) upon addition of the complexes to the ct-DNA. Again, the ΔT_m values suggest primarily groove binding nature of **1** and **2** and partial intercalative mode of binding of the pyrenyl complexes to ct-DNA. Viscosity measurements were carried out to examine the effect of the complexes on the specific relative viscosity of the ct-DNA which gave a measure on the increase in its contour length associated with the separation of the DNA base pairs caused by intercalation. The viscosity data also indicate groove binding nature of **1** and **2** and partial intercalation of **3** and **4** to the ct-DNA.

We have studied the DNA photocleavage activity of the complexes using supercoiled pUC19 DNA in Tris-HCl/NaCl (50 mM, pH = 7.2) buffer using green and red light of 568 and 785 nm wavelength that were chosen based on the MLCT band of the complexes **1–3**. The ferrocenyl complexes (40 μ M) showed significant cleavage of SC DNA giving $\sim 80\%$ nicked circular (NC) DNA in red light (Fig. 8, Table 4). Complex **4** lacking the ferrocenyl moiety is less active in light of 568 nm. Control experiments using only DNA in light or the complexes in dark did not show any significant DNA cleavage activity. The complexes in red light of 785 nm showed efficient photocleavage of DNA giving $\sim 70\%$ NC DNA formation. Mechanistic studies were carried out using complex **3** in the presence of various additives to explore any formation of reactive oxygen species. The complex did not show any DNA photocleavage activity under an argon atmosphere indicating possible involvement of ROS like singlet oxygen and/or hydroxyl radicals. Singlet oxygen quenchers, viz. sodium azide and TEMP did not show any inhibition of the DNA photocleavage activity and addition of D_2O in which singlet oxygen has longer life time did not show any enhancement in the DNA photocleavage activity, thus ruling out any singlet oxygen formation [48]. The hydroxyl radical scavengers, viz. DMSO, KI and catalase exhibited significant inhibitory effect on the DNA photocleavage activity suggesting the formation of hydroxyl radical ($\cdot OH$) as the ROS. Superoxide dismutase (SOD) showed only partial inhibitory effect and this could be due to spontaneous dismutation of superoxide radical anion to the $\cdot OH$ radicals.

Table 4
Selected SC pUC19 DNA (0.5 μ g) cleavage data for complexes **1–4**.

Reaction conditions ^a	%NC ^b form $\lambda = 568$ nm	%NC ^b form $\lambda = 785$ nm
DNA control	2	3
DNA + [VO(Fc-tpy)(acac)](ClO ₄) (1)	56	46
DNA + [VO(Fc-tpy)(nap-acac)](ClO ₄) (2)	70 ^c	62
DNA + [VO(Fc-tpy)(py-acac)](ClO ₄) (3)	88 ^d	76
DNA + [VO(Ph-tpy)(py-acac)](ClO ₄) (4)	26 ^e	70

^a In Tris-buffer medium (pH = 7.2).

^b NC = nicked circular form of pUC19 DNA. λ , laser wavelength. Photo-exposure time (t) = 2 h. Concentration of complexes **1–4** was 40 μ M for 568 nm and 50 μ M for 785 nm experiment.

^c The ligand Hnap-acac alone gave 5% NC form at this wavelength.

^d The ligand Hpy-acac alone gave 8% NC form at this wavelength.

^e No visible band was observed at this wavelength for this complex.

3. Conclusions

Ferrocenyl-terpyridyl oxovanadium(IV) complexes of acetylacetonate derivatives having pendant fluorophores are designed, synthesized, characterized and their DNA photocleavage and visible light-induced cytotoxic activity studied. The ferrocenyl complexes show significant DNA photocleavage activity compared to its phenyl analogue. Mechanistic study revealed formation of hydroxyl radicals as the reactive oxygen species. The complexes show high cellular uptake. They are remarkably PDT active in MCF-7 cells compared to HeLa cells on photo-excitation of their MLCT band. The positive effect of the ferrocenyl moiety is evidenced from a four-fold increase in photocytotoxicity of the ferrocenyl complex **3** compared to its phenyl analogue **4**. The IC_{50} value of complex **3** in light in MCF-7 cells is similar to that of Photofrin[®]. The ferrocenyl complex **3** showed ~ 4 -fold increase in cellular uptake compared to its phenyl analogue **4** and this could be due to the lipophilic nature of the ferrocenyl moiety. The fluorescence property of the naphthyl and pyrenyl moieties in the complexes is used for cellular imaging which showed localization of the complex predominantly in the cytosol and partially in the nucleus of the HeLa and MCF-7 cells. The photocytotoxicity of the acetylacetonate derivatives compares well with their reported curcumin analogues. The light-induced cell death by the complexes proceeds via an apoptotic pathway. The results are of importance toward developing ferrocenyl conjugates of transition metals as potential metal-based photocytotoxic agents.

4. Experimental

4.1. Materials and methods

The reagents and chemicals were procured from commercial sources (s.d. Fine Chemicals, India; Sigma–Aldrich, USA) and used without further purifications. Solvents were purified by standard procedures prior to use [49]. Synthesis of the complexes was performed by standard Schlenk technique under nitrogen atmosphere. Supercoiled (SC) pUC19 DNA (cesium chloride purified) was purchased from Bangalore Genie (India). Ferrocenecarboxaldehyde, acetyl naphthalene, pyrene, sodium perchlorate, 5,5-dimethyl-1-pyrroline 1-oxide (DMPO), calf thymus (ct) DNA, agarose (molecular biology grade), catalase, superoxide dismutase (SOD), 2,2,6,6-tetramethyl-4-piperidone (TEMP), MTT (3-(4,5-dimethylthiazole-2-yl)-2,5-diphenyltetrazolium bromide) and ethidium bromide (EB) were purchased from Sigma–Aldrich (USA). Tris(hydroxymethyl)aminomethane-HCl (Tris–HCl) buffer solution

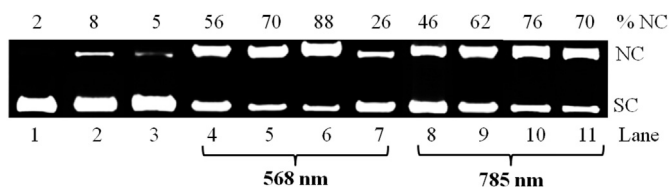


Fig. 8. Cleavage of SC pUC19 DNA (0.2 μ g, 30 μ M) by ligands (Hnap-acac, Hpy-acac) and complexes **1–4** (30 μ M) and ligands (30 μ M) in 50 mmol Tris-HCl/NaCl buffer (pH = 7.2) containing 10% DMF on photo-irradiation with light of 568 nm and 785 nm wavelengths (2 h exposure): lane 1, DNA control; lane 2, DNA + Hpy-acac; lane 3, DNA + Hnap-acac; lanes 4–7, DNA + **1–4** (40 μ M, 568 nm); lanes 8–11, DNA + **1–4** (50 μ M, 785 nm), respectively. SC and NC are the supercoiled and nicked circular forms of the DNA.

was prepared using deionized and sonicated triple-distilled water. The ligands 4'-ferrocenyl-2,2':6',2''-terpyridine (Fc-tpy) and phenylterpyridine (Ph-tpy), acetylacetonone derivatives viz., Hnap-acac, Hpy-acac were prepared according the literature procedures [31,32].

4.2. General methods

The elemental analysis was done using a Thermo Finnigan FLASH EA 1112 CHNS analyzer. The electronic, infrared and emission spectra were recorded on Perkin–Elmer Lambda 650, Perkin–Elmer spectrum one 55 and Horiba Jobin Yvon max4 spectrometer, respectively. Molar conductivity measurements were carried out using a Control Dynamics (India) conductivity meter. Cyclic voltammetric measurements were made at room temperature on an EG&G PAR 253 VersaStat potentiostat/galvanostat using a three electrode configuration consisting of a glassy carbon working, platinum wire auxiliary and saturated calomel reference electrode (SCE) with 0.1 M tetrabutylammonium perchlorate as a supporting electrolyte. Electrospray ionization (ESI) mass spectral measurements were made using Bruker Daltonics make Esquire 300 Plus ESI model. Magnetic measurements were done in the solid state at 25 °C using a magnetic susceptibility balance, Sherwood Scientific, Cambridge, UK.

CAUTION: Perchlorate salts being potentially explosive, only small quantity of the sample was used with due precautions.

4.3. Synthesis of the complexes 1–4

VOSO₄ (0.16 g, 1.0 mmol) was dissolved in 1.0 ml of ethanol and to this was added BaCl₂·2H₂O (0.244 g, 1.0 mmol) taken in 1.0 ml of ethanol and the mixture was stirred for 1.0 h at 25 °C. The mixture was centrifuged to remove precipitated barium sulphate. The clear solution was separated and to this was added the acetylacetonone derivative (1.0 mmol; Hacac, 0.01 g; Hnap-acac, 0.21 g; Hpy-acac, 0.27 g), previously neutralized with NaOH (0.04 g in 1.0 ml water). The solution was stirred for 30 min. To this solution was added Fc-tpy or Ph-tpy dissolved in CHCl₃:MeOH (1:4 v/v, 5.0 ml) to get a dark blue solution on stirring for an additional 30 min. The complex was precipitated as its perchlorate salt by adding an excess of aqueous NaClO₄. The precipitate was isolated and washed with cold methanol and diethyl ether followed by drying in vacuum. The ferrocenyl complexes 1–3 were navy blue coloured amorphous solids, while the phenyl complex 4 was golden yellow coloured amorphous solid.

4.3.1. [VO(Fc-tpy)(acac)](ClO₄) (1)

Yield: 69%. Anal. Calcd for C₃₀H₂₆N₃O₇ClFeV: C, 52.77; H, 3.84; N, 6.15. Found: C, 52.50; H, 3.78; N, 6.10. ESI-MS (*m/z*) in MeCN: 583 [M-(ClO₄)]⁺. Λ_M in DMF: 84 S m² M⁻¹. UV–Vis in DMF–Tris HCl buffer (1:1 v/v) [λ_{max} , nm (ϵ , dm³ M⁻¹ cm⁻¹): 581 (2608), 427 (1025), 334 (10080), 287 (15175)]. FT-IR (cm⁻¹): 3424br, 3082w, 1610s, 1564s, 1516s, 1477s, 1435m, 1373s, 1290w, 1250m, 1096vs (ClO₄), 1041m, 1026m, 958s (V=O), 902w, 830w, 794m, 766w, 732m, 700w, 676w, 660w, 623m, 570w, 555w, 515w, 478w (br, broad; vs, very strong; s, strong; m, medium; w, weak). μ_{eff} = 1.65 μ_B at 298 K.

4.3.2. [VO(Fc-tpy)(nap-acac)](ClO₄) (2)

Yield: 79%. Anal. Calcd for C₃₉H₃₀N₃O₇ClFeV: C, 58.93; H, 3.80; N, 5.29. Found: C, 58.82; H, 3.71; N, 5.20. ESI-MS (*m/z*) in MeCN: 695 [M-(ClO₄)]⁺. Λ_M in DMF: 86 S m² M⁻¹. UV–Vis in DMF–Tris HCl buffer (1:1 v/v) [λ_{max} , nm (ϵ , dm³ M⁻¹ cm⁻¹): 583 (3014), 425 (1285), 330 (13175), 293 (17930)]. FT-IR (cm⁻¹): 3420br, 3074w, 2922w, 1709m, 1612s, 1556s, 1516s, 1480s, 1460w, 1436m, 1376s,

1290w, 1255w, 1223w, 1143w, 1095w, 1095vs (ClO₄), 1032m, 958s (V=O), 911w, 878w, 788m, 751w, 674w, 623m, 573w, 514w, 474w. μ_{eff} = 1.68 μ_B at 298 K.

4.3.3. [VO(Fc-tpy)(py-acac)](ClO₄) (3)

Yield: 72%. Anal. Calcd for C₄₅H₃₂N₃O₇ClFeV: C, 62.20; H, 3.71; N, 4.84. Found: C, 62.42; H, 3.78; N, 4.72. ESI-MS (*m/z*) in MeCN: 769 [M-(ClO₄)]⁺. Λ_M in DMF: 79 S m² M⁻¹. UV–Vis in DMF–Tris HCl buffer (1:1 v/v) [λ_{max} , nm (ϵ , dm³ M⁻¹ cm⁻¹): 586 (3536), 396 (9465), 368sh (16220), 346 (20160), 286 (35430) (sh, shoulder)]. FT-IR (cm⁻¹): 3441br, 3074w, 1610s, 1563s, 1536sm, 1517w, 1499m, 1451m, 1460w, 1435m, 1388m, 1372m, 1324w, 1267w, 1255w, 1096vs (ClO₄), 1031m, 963s (V=O), 856w, 848w, 791m, 822w, 771wm 714w, 670w, 625m, 579w, 542w, 517w, 478w. μ_{eff} = 1.62 μ_B at 298 K.

4.3.4. [VO(Ph-tpy)(py-acac)](ClO₄) (4)

Yield: 74%. Anal. Calcd for C₄₁H₂₈N₃O₇ClV: C, 64.70; H, 3.71; N, 5.52. Found: C, 64.58; H, 3.78; N, 5.40. ESI-MS (*m/z*) in MeCN: 661 [M-(ClO₄)]⁺. Λ_M in DMF: 74 S m² M⁻¹. UV–Vis in DMF–Tris HCl buffer (1:1 v/v) [λ_{max} , nm (ϵ , dm³ M⁻¹ cm⁻¹): 777 (90), 392sh (7896), 358 (11820), 280 (47850)]. FT-IR (cm⁻¹): 3451br, 3072w, 1608s, 1561s, 1526sm, 1491m, 1441m, 1434m, 1372m, 1324w, 1263w, 1255w, 1095vs (ClO₄), 1032m, 961s (V=O), 851w, 791m, 822w, 710w, 672w, 622m, 532w, 482w. μ_{eff} = 1.65 μ_B at 298 K.

4.4. Solubility

The complexes were soluble in acetonitrile, chloroform, dichloromethane, dimethyl sulfoxide (DMSO), dimethylformamide (DMF) and 1% DMSO-DMEM media. They were sparingly soluble in water.

4.5. Computational methodology

All calculations were performed using GAUSSIAN09 program suite and the geometries of the complexes were optimized at B3LYP/6-31g (d,p) level of theory [35–37]. Details are given as Supporting Information. Time-dependent density functional theory (TD-DFT) calculations were carried out to investigate the optical properties of the complexes in DMF. The lowest 40 transitions up to 400 nm were taken into account in the calculations of the absorption spectra. Molecular orbital (MO) compositions were calculated using the Multiwfn program [50].

4.6. Cell culture

HeLa (human cervical carcinoma), MCF-7 (human breast adenocarcinoma), 3T3 (standard normal fibroblast) cells were maintained in Dulbecco's Modified Eagle's Medium (DMEM) supplemented with 10% fetal bovine serum (FBS), 100 IU ml⁻¹ of penicillin, 100 mg ml⁻¹ of streptomycin and 2 mM of Glutamax at 37 °C in a humidified incubator at 5% CO₂. The adherent cultures were grown as monolayer and were passaged once in 4–5 days by exposure to 0.25% Trypsin-EDTA.

4.7. Cellular experiments

4.7.1. Cytotoxicity of the complexes

The cytotoxicity of the complexes in HeLa and MCF-7 cells was assessed by MTT assay [51]. About 1 × 10⁴ cells were seeded into 96-well plates in 100 μ L media per well. The cells were allowed to grow for 24 h in a CO₂ incubator at 37 °C. Different concentrations of the complexes dissolved in 1% DMSO were added to the cells. Incubation was continued for a further period of 4 h at 37 °C in the

CO₂ incubator. After incubation, the medium was replaced with PBS and photo-irradiation was performed for 1 h in visible light of 400–700 nm using Luzchem Photoreactor (Model LZC-1, Ontario, Canada; light fluence rate: 2.4 mW cm⁻²; light dose = 10 J cm⁻²). For experiment using NAC as a ROS scavenger, photo-irradiation was done in presence of 0.5 mM NAC containing PBS. Post irradiation, PBS was replaced with 10% DMEM and cells were cultured for a further period of 20 h in dark followed by addition of 25 µL of 4 mg ml⁻¹ of MTT to each well and incubated for an additional 3 h. The culture medium was discarded and a 200 µL volume of DMSO was added to dissolve the purple formazan crystals. The absorbance at 540 nm was determined using an ELISA microplate reader (BioRad, Hercules, CA, USA). Cytotoxicity of the test compounds was measured as the percentage ratio of the absorbance of the treated cells to the untreated controls. The IC₅₀ values were determined by nonlinear regression analysis (GraphPad Prism 5).

4.7.2. Cellular uptake by ICP-MS

Uptake of the oxovanadium(IV) complexes was determined by measuring the cellular vanadium content using ICP-MS. HeLa and MCF-7 cells (~0.5 × 10⁶ cells) were grown in 6 wells plate and incubated at 37 °C under 5% CO₂ atmosphere for overnight. The culture medium was removed and replaced with a medium containing the complex (30 µM). After incubation for 4 h, the medium was removed, washed twice with 3 ml PBS to remove any excess complex from the extracellular media, trypsinized and digested in concentrated nitric acid (65% HNO₃) at 70 °C for 2 h. Dilution was done with Milli-Q water to the final volume of 10 ml and analysed for ICP-MS. The instrument was calibrated for vanadium using standard solutions containing 1, 10, 100 and 1000 ppb vanadium.

4.7.3. Measurement of intracellular ROS from DCFDA assay

Cell permeable DCFDA when oxidized by cellular ROS is known to generate fluorescent DCF having an emission maximum at 528 nm [52]. To determine the intracellular ROS, ~0.5 × 10⁶ HeLa cells were incubated with the complexes (10 µM) for 4 h in dark. The media was replaced with PBS followed by photo-irradiation for 1 h in serum free conditions. The cells were harvested by trypsinization and a single cell suspension was made. The cells were washed with PBS to remove any extracellular complex and treated with 1 µM DCFDA solution in DMSO and incubated in dark for 30 min at room temperature. The intracellular fluorescence of DCF was monitored by flow cytometry in the FL-1 channel. Control experiments were performed for (a) untreated cells, in order to determine the contribution from auto-fluorescence of cells and (b) cells treated with DCFDA only. Hydrogen peroxide treated cells were taken as a positive control.

4.7.4. Cellular uptake from fluorescence microscopy

The emissive property of the complexes **2** and **3** was utilized to study the cellular localization of the complexes using fluorescence microscopy. HeLa cells (~3 × 10⁴) were grown on glass cover slips in each 6 well plate for 24 h. The cells were subsequently treated with the complexes (10 µM) for 2 and 4 h in dark. Cells were then washed with PBS to remove any extracellular complex and fixed with 4% formaldehyde for 10 min at room temperature. This was followed by incubation with propidium iodide (PI) staining solution (50 µg ml⁻¹ RNase A, 20 µg ml⁻¹ PI in PBS) for 1 h at 42 °C. The cells were washed free of excess PI, mounted in 90% glycerol solution containing Mowiol, an anti-fade reagent, and sealed. Images were acquired using Apotome.2 fluorescence microscope (Carl Zeiss, Germany) using an oil immersion lens at 63× magnification. The images were analyzed using the AxioVision Rel 4.9.1 (Carl Zeiss, Germany) software. Similarly, to view the PDT effect, cells treated with complexes **3** and **4** were plated on glass cover-slip and

exposed to visible light for 1 h and images were captured.

4.8. EPR spin trap with DMPO

EPR spectra were recorded at room temperature using a Bruker ESP 300 EPR spectrometer at 9.5 GHz (X-band) employing 100 kHz field modulation. EPR measurements for the oxovanadium(IV) complexes were done in 4 mM DMF solution at 25 °C. For spin-trapping •OH, the sample solution containing complex **4** (100 µL, 1 mM), DMPO (100 µL, 0.5 M) and 800 µL phosphate buffer was photo-irradiated with visible light for 30 min. The solution was then transferred to an EPR quartz capillary tube to record the spectra at 25 °C. The g values were estimated using solid DPPH as an internal standard (g = 2.0036).

4.9. DNA binding and cleavage experiments

The ct-DNA binding experiments were done in Tris–HCl/NaCl buffer (5 mM Tris–HCl, 5 mM NaCl, pH = 7.2) or phosphate buffer (pH = 7.4) using DMF solution of the complexes **1–4** following reported procedures [53,54]. DNA photocleavage studies were carried out using DMF solutions of the complexes and supercoiled pUC19 DNA in 50 mM Tris–HCl buffer containing 50 mM NaCl. The DNA photocleavage studies were carried out in visible light of 568 nm of 50 mW laser power using a Spectra Physics Water-Cooled Mixed-Gas Ion Laser Stabilite® 2018-RM (continuous-wave (CW) beam diameter at 1/e² = 1.8 mm ± 10% and beam divergence with full angle = 0.7 mrad ± 10%) and in near IR 785 nm from a diode laser (100 mW laser power, Model LQC785-100C from Spectra Physics with LD module) [55]. Appropriate controls were used for all the experiments and suitable inhibitors were used for mechanistic investigations, as described above.

Acknowledgments

We thank the Department of Science and Technology (DST), Government of India, and the Council of Scientific and Industrial Research (CSIR), New Delhi, for financial support (CSIR No. 01(2559)/12/EMR-II and DST No. SR/S5/MBD-02/2007). We are thankful to the Alexander von Humboldt Foundation, Germany, for donation of an electroanalytical system. A.R.C. thanks DST for J.C. Bose national fellowship. We thank Prof. S.V. Bhat and Mrs. S.K. Bhagyashree for assistance in the EPR experiments and Dr. R. Chakrabarti for the ICP-MS facility. We thank the Department of Biotechnology (DBT) for the FACS facility. S.P. thanks SERC of our institute for the computational facility.

Appendix A. Supplementary data

Supplementary data related to this article can be found at <http://dx.doi.org/10.1016/j.ejmech.2015.01.003>.

References

- [1] M. Ethirajan, Y. Chen, P. Joshi, R.K. Pandey, *Chem. Soc. Rev.* **40** (2011) 340–362.
- [2] J.P. Celli, B.Q. Spring, I. Rizvi, C.L. Evans, K.S. Samkoe, S. Verma, B.W. Pogue, T. Hasan, *Chem. Rev.* **110** (2010) 2795–2838.
- [3] P. Agostinis, K. Berg, K.A. Cengel, T.H. Foster, A.W. Girotti, S.O. Gollnick, S.M. Hahn, M.R. Hamblin, A. Juzeniene, D. Kessel, M. Korbelik, J. Moan, P. Mroz, D. Nowis, J. Piette, B.C. Wilson, J. Golab, *CA Cancer J. Clin.* **61** (2011) 250–281.
- [4] R. Bonnett, *Chemical Aspects of Photodynamic Therapy*, Gordon & Breach, London, 2000.
- [5] P. Couleaud, V. Morosini, C. Frochot, S. Richeter, L. Raehm, J.-O. Durand, *Nanoscale* **2** (2010) 1083–1095.
- [6] M.J. Ochsner, *Photochem. Photobiol.* **32** (1996) 3–9.
- [7] S.I. Moriwaki, J. Misawa, Y. Yoshinari, I. Yamada, M. Takigawa, Y. Tokura, *Photodermatol. Photoimmunol. Photomed.* **17** (2001) 241–243.

- [8] U. Schatzschneider, *Eur. J. Inorg. Chem.* (2010) 1451–1467.
- [9] X. Jia, F.F. Yang, J. Li, J.Y. Liu, J.P. Xue, *J. Med. Chem.* 56 (2013) 5797–5805.
- [10] N.J. Farrer, L. Salassa, P.J. Sadler, *Dalton Trans.* (2009) 10690–10701.
- [11] E. Ranyuk, N. Cauchon, K. Klarskov, B. Guérin, J.E. van Lier, *J. Med. Chem.* 56 (2013) 1520–1534.
- [12] M.A. Sgambellone, A. David, R.N. Garner, K.R. Dunbar, C. Turro, *J. Am. Chem. Soc.* 135 (2013) 11274–11282.
- [13] P. Prasad, I. Khan, P. Kondaiah, A.R. Chakravarty, *Chem. Eur. J.* 19 (2013) 17445–17455.
- [14] N.L. Fry, P.K. Mascharak, *Acc. Chem. Res.* 44 (2011) 289–298.
- [15] A.R. Chakravarty, M. Roy, *Prog. Inorg. Chem.* 57 (2012) 119–202.
- [16] C.J. Burrows, J.G. Muller, *Chem. Rev.* 98 (1998) 1109–1151.
- [17] K. Szacitowski, W. Macyk, A. Drzewiecka-Matuszek, M. Brindell, G. Stochel, *Chem. Rev.* 105 (2005) 2647–2694.
- [18] B. Balaji, B. Banik, P.K. Sasmal, B. Maity, R. Majumdar, R.R. Dighe, A.R. Chakravarty, *Eur. J. Inorg. Chem.* (2012) 126–135.
- [19] T.K. Goswami, S. Gadadhar, M. Roy, M. Nethaji, A.A. Karande, A.R. Chakravarty, *Organometallics* 31 (2012) 3010–3021.
- [20] B. Maity, M. Roy, B. Banik, R. Majumdar, R.R. Dighe, A.R. Chakravarty, *Organometallics* 29 (2010) 3632–3641.
- [21] E. Hillard, A. Vessières, L. Thouin, G. Jaouen, C. Amatore, *Angew. Chem. Int. Ed.* 45 (2006) 285–290.
- [22] C. Ornelas, *New J. Chem.* 35 (2011) 1973–1985.
- [23] G. Gasser, I. Ott, N. Metzler-Nolte, *J. Med. Chem.* 54 (2011) 3–25.
- [24] J. Manosroi, K. Rueanto, K. Boonpisuttinant, W. Manosroi, C. Biot, H. Akazawa, T. Akihisa, W. Issarangporn, A. Manosroi, *J. Med. Chem.* 53 (2010) 3937–3943.
- [25] F. Dubar, G. Anquetin, B. Pradines, D. Dive, J. Khalife, C. Biot, *J. Med. Chem.* 52 (2009) 7954–7957.
- [26] D. Dive, C. Biot, *ChemMedChem* 3 (2008) 383–391.
- [27] D. Osella, M. Ferrali, P. Zanello, F. Laschi, M. Fontani, C. Nervi, G. Cavignolo, *Inorg. Chim. Acta* 306 (2000) 42–48.
- [28] B. Balaji, B. Balakrishnan, S. Perumalla, A.A. Karande, A.R. Chakravarty, *Eur. J. Med. Chem.* 85 (2014) 458–467.
- [29] B. Balaji, K. Somyajit, B. Banik, G. Nagaraju, A.R. Chakravarty, *Inorg. Chim. Acta* 400 (2013) 142–150.
- [30] M.A. Tomren, M. Måsson, T. Loftsson, H.H. Tønnesen, *Int. J. Pharm.* 338 (2007) 27–34.
- [31] E.C. Constable, A.J. Edwards, R. Martínez-Máñez, P.R. Raithby, A.M.W.C. Thompson, *J. Chem. Soc. Dalton Trans.* (1994) 645–650.
- [32] D.F. Evans, *J. Chem. Soc.* (1961) 1987–1993.
- [33] P.K. Sasmal, R. Majumdar, R.R. Dighe, A.R. Chakravarty, *Dalton Trans.* 39 (2010) 7104–7113.
- [34] K. Hutchison, J.C. Morris, T.A. Nile, J.L. Walsh, *Inorg. Chem.* 38 (1999) 2516–2523.
- [35] M.J. Frisch, et al., *Gaussian 03, Revision B.4*, Gaussian Inc., Pittsburgh, PA, 2003 (vide Supplementary data for full reference).
- [36] A.D. Becke, *J. Chem. Phys.* 98 (1993) 5648–5652.
- [37] C. Lee, W. Yang, R.G. Parr, *Phys. Rev. B* 37 (1988) 785–789.
- [38] P.K. Sasmal, S. Saha, R. Majumdar, S. De, R.R. Dighe, A.R. Chakravarty, *Dalton Trans.* 39 (2010) 2147–2158.
- [39] E. Delaey, F. Van Larr, D. De Vos, A. Kamuhabwa, P. Jacobs, P. De Witte, *J. Photochem. Photobiol. B* 55 (2000) 27–36.
- [40] F. Ménard, V. Sol, C. Ringot, R. Granet, S. Alves, C.L. Morvan, Y. Queneau, N. Ono, P. Krausz, *Bioorg. Med. Chem.* 17 (2009) 7647–7657.
- [41] S. Saha, D. Mallick, R. Majumdar, M. Roy, R.R. Dighe, E.D. Jemmis, A.R. Chakravarty, *Inorg. Chem.* 50 (2011) 2975–2987.
- [42] I. Ott, K. Schmidt, B. Kircher, P. Schumacher, T. Wigienda, R. Gust, *J. Med. Chem.* 48 (2005) 622–629.
- [43] S.Y. Sun, *Cancer Biol. Ther.* 9 (2010) 109–110.
- [44] G.M. Pieper, C.C. Felix, B. Kalyanaraman, M. Turk, A.M. Roza, *Free Radic. Biol. Med.* 19 (1995) 219–225.
- [45] M. Hoebeke, H.J. Schuitmaker, L.E. Jannink, T.M.A.R. Dubbelman, A. Jakobs, A.V. Vorst, *Photochem. Photobiol.* 66 (1997) 502–508.
- [46] B. Maity, B.V.S.K. Chakravarthi, M. Roy, A.A. Karande, A.R. Chakravarty, *Eur. J. Inorg. Chem.* (2011) 1379–1386.
- [47] G. Tabbi, C. Cassino, G. Cavignolo, D. Colangelo, A. Ghiglia, I. Viano, D. Osella, *J. Med. Chem.* 45 (2002) 5786–5796.
- [48] P.B. Merkel, D.R. Kearns, *J. Am. Chem. Soc.* 94 (1972) 1029–1030.
- [49] D.D. Perrin, W.L.F. Armarego, D.R. Perrin, *Purification of Laboratory Chemicals*, Pergamon Press, Oxford, 1980.
- [50] T. Lu, F. Chen, *J. Comput. Chem.* 33 (2012) 580–592.
- [51] T. Mosmann, *J. Immunol. Methods* 65 (1983) 55–63.
- [52] A. Gomes, E. Fernandes, J.L.F.C. Lima, *J. Biochem. Biophys. Methods* 65 (2005) 45–80.
- [53] J.D. McGhee, P.H. von Hippel, *J. Mol. Biol.* 86 (1974) 469–489.
- [54] M.T. Carter, M. Rodriguez, A.J. Bard, *J. Am. Chem. Soc.* 111 (1989) 8901–8911.
- [55] P.K. Sasmal, S. Saha, R. Majumdar, R.R. Dighe, A.R. Chakravarty, *Inorg. Chem.* 49 (2010) 849–859.